A Comparative Study of Fracture Behavior Between Carbon Black/Poly(ethylene terephthalate) and Multiwalled Carbon Nanotube/Poly(ethylene terephthalate) Composite Films

Haruki Kobayashi,[1] Masatoshi Shioya,[1] Tomoya Tanaka,[1] Toshihira Irisawa,[1] Shinichi Sakurai,[2] Katsuhiro Yamamoto[3]

[1]Department of Organic and Polymeric Materials, Tokyo Institute of Technology, Megro-Ku, Tokyo 152-8552, Japan
[2]Graduate School of Science and Technology, Kyoto Institute of Technology, Matsugasaki, Sakyo-Ku, Kyoto 606-8585, Japan
[3]Graduate School of Engineering, Nagoya Institute of Technology, Gokiso-Cho, Showa-Ku, Nagoya 466-8555, Japan

ABSTRACT: Fracture behavior of amorphous poly(ethylene terephthalate) (PET) films added multiwalled carbon nanotube (MWCNT) has been compared with that of the PET films added with carbon black (CB) to elucidate the effects of the large aspect ratio of MWCNT. Fracture toughness has been evaluated using the essential work of fracture tests. Evolution of the crazes has been analyzed by conducting time-resolved small-angle X-ray scattering measurements during tensile deformation of the films at room temperature using synchrotron radiation. CB and MWCNT increased the fracture toughness of the PET film by increasing the plastic work of fracture. This resulted from the effects of the fillers to prevent the localization of deformation upon the crazes formed at earlier stages of tensile deformation and to retard the growth of the fibrils in the crazes to a critical length. The CB particles provided a number of sites where the crazes were preferably formed due to stress concentration. In the case of MWCNT, on the other hand, the widening of the crazes formed at earlier stages was suppressed due to the bridging effect arising from the large aspect ratio of MWCNT. © 2007 Wiley Periodicals, Inc. J Appl Polym Sci 106: 152–160, 2007

Key words: polymer composite materials; carbon nanotube; poly(ethylene terephthalate); mechanical property; small-angle X-ray scattering

INTRODUCTION

Mechanical properties of polymers such as tensile strength, modulus, and fracture toughness can be increased by dispersing various kinds of fillers. Among the fillers, carbon nanotube (CNT), having a large aspect ratio, is expected to exert reinforcing effects, which have not been obtained with the conventional micrometer scale fillers. It has been shown both theoretically[1–3] and experimentally[4–6] that CNT has exceptionally high tensile strength and modulus. Treacy et al.[4] have estimated Young's modulus of multiwalled carbon nanotube (MWCNT) as 1.8 TPa by measuring the amplitude of its intrinsic thermal vibrations using transmission electron microscope (TEM). Wong et al.[5] have estimated the modulus of MWCNT as 1.28 TPa by measuring the bending force, using atomic force microscope (AFM). Yu et al.[6] have carried out the tensile test of individual MWCNT by attaching both ends of MWCNT to the AFM cantilever probes under observation with scanning electron microscope (SEM). They estimated the modulus of MWCNT as 270–950 GPa and the tensile strength as 20–63 GPa. A number of studies have been conducted on the mechanical properties of CNT/polymer composites. Various polymers such as polystyrene,[7,8] polycarbonate,[9] polyethylene,[10] poly(methyl methacrylate),[11] poly(vinyl alchol),[12] polyacrylonitrile,[13] poly (ethylene terephthalate) (PET),[14] polyimide,[15] and epoxy resin[16–18] have been tested as the matrix polymer and various mechanical properties such as tensile and bending strengths and moduli, yield stress, fracture toughness, fatigue, and friction have been investigated. Carbon black (CB), which is also the nanometer scale filler but with the aspect ratio of about unity, is known to increase the fracture toughness of polymers.[18,19] This study aims at elucidating the effects of the large aspect ratio of CNT on the fracture behavior of a CNT/polymer composite by conducting in situ observation of structure changes of the composite during deformation.

The observations using SEM, TEM, and AFM have been carried out in the studies of structure and

morphology for polymer materials as reviewed by Mark[20] and for CNT/polymer composites as reported by various researchers.[7,9,13,17,18] Although the TEM observation is a quite effective method to directly observe nanometer scale structure, its drawback is that the specimen thickness should be less than some tens of nanometers, which is comparable with the diameter of CNT. The stress state around CNT in these thin specimens under deformation differs from that in the bulk specimen. In this study, therefore, structural changes of the CNT/polymer composite during deformation will be measured using small-angle X-ray scattering (SAXS). The evolution of crazes during deformation of PET has been detected with SAXS.[14,21,22] We have investigated the formation, widening, and fracture processes of the crazes in a CNT/amorphous PET composite film by conducting time-resolved SAXS measurements during tensile deformation, using synchrotron radiation.[14]

In many polymers, the crazes are developed during tensile deformation and act as the precursor of the cracks leading to the macroscopic fracture of the polymers. The crazes, however, have the load bearing capability unlike true cracks due to the internal fibrils aligned in parallel to the loading direction. Therefore, when the crazes grow stably during tensile deformation, they dissipate energy and contribute to the increase in the fracture toughness. The fibrils in the crazes break when their length reached to a certain critical length[23] and the crazes turn into true cracks. Thus, the evolution of the crazes governs the fracture behavior such as fracture toughness of polymers.[24,25]

In this study, the fracture toughness and the evolution of the crazes of MWCNT/PET composite films have been compared with those of CB/PET composite films. The essential work of fracture (EWF) tests has been conducted to evaluate the fracture toughness. The time-resolved SAXS measurements using synchrotron radiation have been performed during tensile deformation of the films at room temperature to detect the evolution of the crazes.

EXPERIMENTAL

Specimens

Neat PET films, CB/PET composite films, and MWCNT/PET composite films were prepared using PET with an intrinsic viscosity of 1.07 dL g^{-1} and a density of 1.41 g cm^{-3} (Unitika SA1206). CB used was furnace black with a diameter of about 25 nm (Mitsubishi Chemical Corp. No. 40). Two types of MWCNTs with a diameter of 20–50 nm and the length of several micrometers supplied from two different producers were used. These MWCNTs will be distinguished as MWCNT-I and MWCNT-II. Because of the limitation of available amount of MWCNT-II, the fracture

toughness tests were conducted only for MWCNT-I/PET composite films.

The neat PET films, CB/PET composite films, and MWCNT/PET composite films were prepared as follows: First, desired amounts of the fillers and the PET pellets were mixed so that the weight fractions of the fillers in the composite films varied between 0 and 5 wt %. Second, the mixtures were kneaded with a dual spindle kneader at 280°C for 10 min. To impose the same process history on the neat PET films and the matrix of the composite films, the kneading process with the same conditions as shown earlier was also applied to the PET for preparing the neat films. Third, the kneaded materials were hot-pressed at 280°C into the films and immediately quenched by placing the films between two steel plates cooled with water at room temperature to suppress crystallization. The thicknesses of the films were about 80 and 300 μm. Finally, the films were cut into the test pieces and the notches were introduced with a razor blade for the EWF tests and the SAXS measurements.

EWF test

Fracture toughness of the films was evaluated using the EWF tests.[26–28] This method utilized the double-edge-notched specimens schematically shown in Figure 1(a). The initial ligament lengths, i.e., the separations between the notch tips, were varied from 3 to 17 mm in every 1 mm so that the following requirements are satisfied.

$$kB \leq L \leq \min\left(\frac{D}{3}, 2R_p\right) \quad (1)$$

$$2R_p = \frac{1}{\pi}\left(\frac{Ew_e}{\sigma_y^2}\right) \quad (2)$$

where L is the initial ligament length, D the specimen width, B the specimen thickness, R_p the size of the plastic deformation zone at the crack tip,[27] k a constant between 3 and 5, E the tensile modulus, σ_y the tensile yield stress, and w_e the EWF per unit ligament area. The function $\min(x, y)$ stands for x or y whichever is smaller. The specimen with a gauge length of 50 mm was set on a tensile testing machine and drawn at a crosshead speed of 2 mm min^{-1} at room temperature. The changes of the shape of the specimen during tensile deformation are schematically shown in Figure 1(b).

The principle of EWF method is as follows: the total work of fracture W_t consists of the essential work W_e and the plastic work (nonessential work) W_p. By denoting the total work of fracture dissipated per unit area as w_t, the plastic work dissipated per unit vol-
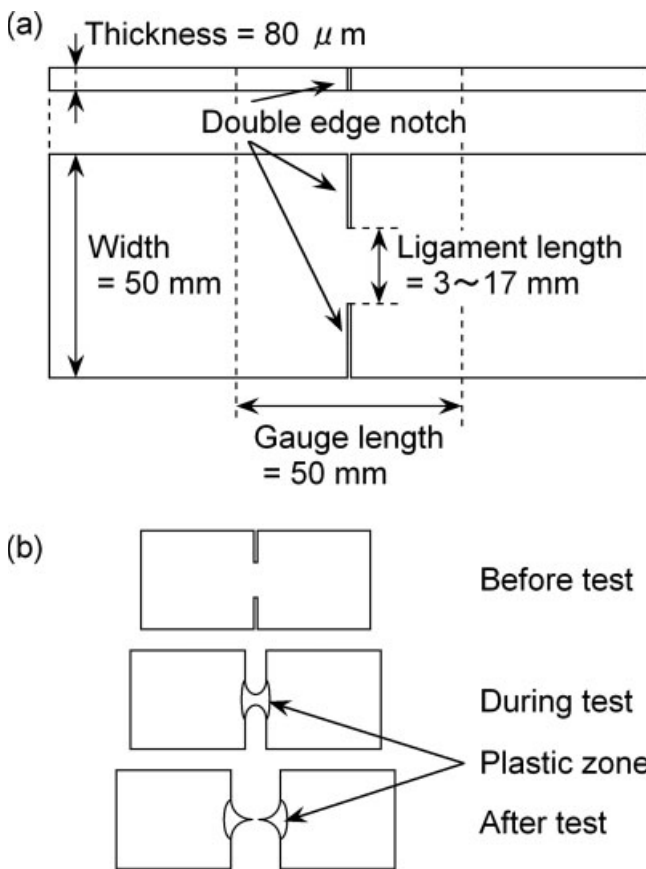
Figure 1 Schematic illustrations of double-edge-notched specimen for EWF tests (a) and changes of shape of specimen during tensile deformation (b).

ume as w_p and the plastic zone shape factor as β, the following expression can be obtained.

$$w_t = \left(\frac{W_t}{BL}\right) = \left(\frac{W_e}{BL}\right) + \left(\frac{W_p}{BL}\right) = w_e + \beta w_p L \quad (3)$$

This equation shows that the intercept and the slope of the regression line fit to the plots of w_t vs. L gives the values of w_e and βw_p.

SAXS

Time-resolved SAXS measurements were carried out during tensile deformation of the films at room temperature using the facility at BL-15A of Photon Factory, High Energy Accelerator Research Organization, Japan. This experiment utilized surface-notched specimens schematically shown in Figure 2(a). The specimen was set on a miniature tensile testing machine (Kato Tech, AK-01) so that the notch was centered between the two grips of the testing machine. The notch stayed at a fixed position during tensile deformation since the two grips were moved at the same velocity in the counter directions. The specimen with an initial gauge length of 10 mm was

stretched up to failure at a deformation speed of 2 μm/s. The changes of the shape of the specimen during tensile deformation are schematically shown in Figure 2(b). During tensile deformation, synchrotron radiation X-ray beam was incident on the notch. The incident X-ray was with a wavelength of 0.15 nm and cross section sizes of 0.2 mm × 0.3 mm. The SAXS patterns were detected with a charge-coupled device camera and an image intensifier as shown in Figure 2(c). The specimen-to-detector length was set to 2.1 m. The time interval between the succeeding measurements of the SAXS patterns was 2 or 5 s and the exposure time for obtaining each pattern was 0.051 or 0.451 s.

WAXD

Wide angle X-ray diffraction (WAXD) of the films was measured without applying tensile deformation at room temperature using a diffractometer, a position sensitive proportional counter, and Ni-filtered
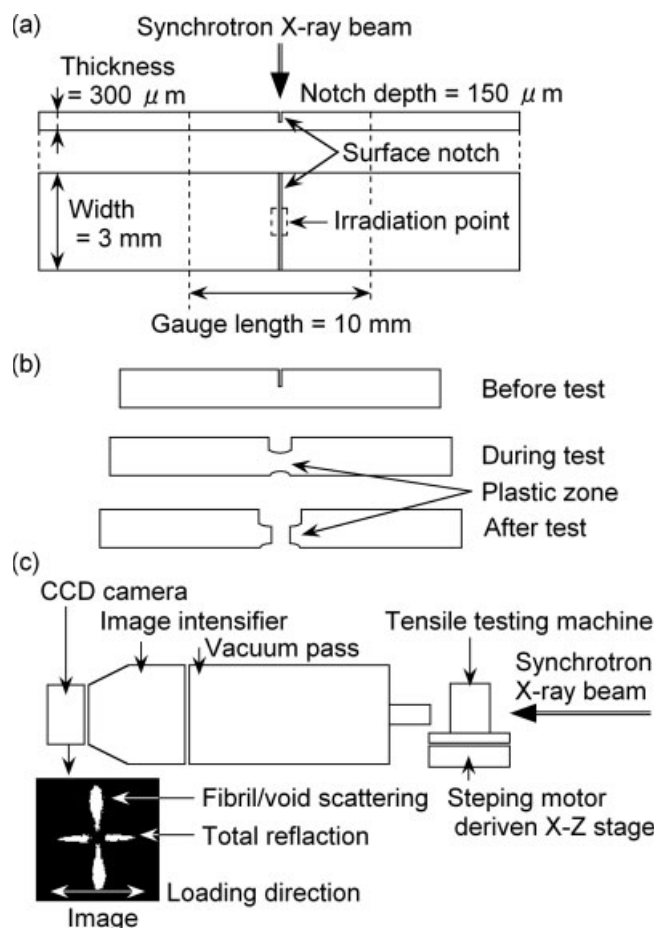

Figure 2 Schematic illustrations of surface-notched specimen for SAXS measurements (a), changes of shape of specimen during tensile deformation (b), and geometry of time-resolved SAXS measurements during tensile deformation (c).
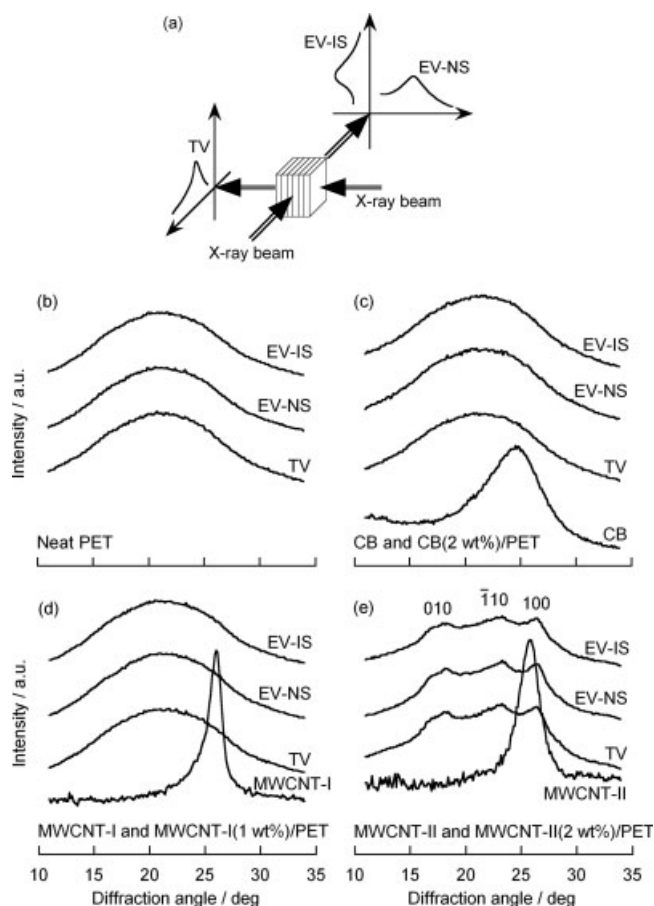
Figure 3 Geometries of WAXD measurements (a), WAXD profiles of neat PET film (b), CB and CB (2 wt %)/PET composite film (c), MWCNT-I and MWCNT-I (1 wt %)/PET composite film (d), and MWCNT-II and MWCNT-II (2 wt %)/PET composite film (e).

Cu Kα radiation at a specimen-to-detector length of 110 mm. The X-ray beam was incident on the films perpendicularly (through-view, TV) and in parallel (edge-view, EV) to the film surface as shown in Figure 3(a). With the edge-view geometry, the diffraction was scanned perpendicularly (edge-view normal-scan, EV-NS) and in parallel (edge-view in-plane-scan, EV-IS) to the film surface. The TV and EV measurements were carried out using the films stacked to different thicknesses suitable for individual measurements.

The crystallinity of the films was calculated from the WAXD intensity distributions measured using the fragmented and randomly oriented films. The crystallinity was calculated using the equation:

$$X_c = \frac{\int I_c(2\theta)d(2\theta)}{\int I(2\theta)d(2\theta)} \qquad (4)$$

where X_c is weight fraction of the crystallites, I the total WAXD intensity distribution, I_c the part of the WAXD intensity distribution caused by the crystalli-

tes, and 2θ the diffraction angle. The integration was carried out in the range of $8.8° < 2\theta < 35.0°$.[29] The crystallinity obtained in this way by performing the integration over a limited region of 2θ and ignoring the distortion is an approximate value.[30]

RESULTS AND DISCUSSION

Crystallinity and crystallite orientation

CB and CNT are known to act as the nucleation agent of crystallization for certain polymers.[31,32] Since the crystallinity and the crystallite orientation can influence the mechanical properties, the WAXD profiles of the films are compared in Figure 3. The neat PET film, CB (2 wt %)/PET composite film and MWCNT-I (1 wt %)/PET composite film show only the amorphous haloes of PET. The MWCNT-II (2 wt %)/PET composite film shows the diffraction peaks of PET crystallites. These peaks, however, are weak and no preferential crystallite orientation is observed. The crystallinity of this film was only about 5 wt %.

Tensile behavior

In this study, tensile tests were carried out using specimens with two different geometries. They were double-edge-notched specimens for the EWF tests and surface-notched specimens for the SAXS measurements. Figure 4(a) shows the load-extension curves of the double-edge-notched specimens at a ligament length of 17 mm for the neat PET film, CB (2 wt %)/PET composite film, and MWCNT-I (2 wt %)/PET composite film. The total work of fracture of the films gets larger in the order of the neat PET film, CB (2 wt %)/PET composite film, and MWCNT-I (2 wt %)/PET composite film and they are 221, 246, and 248 kJ m^{-2}, respectively. Figure 4(b) shows the load-extension curves of the surface-notched specimens of the neat PET film, CB (2 wt %)/PET composite film, and MWCNT-II (2 wt %)/PET composite film. The total work of fracture of the films gets larger in the order of the neat PET film, CB (2 wt %)/PET composite film, and MWCNT-II (2 wt %)/PET composite film, and they are 4.66, 9.76, and 11.03 kJ m^{-2}, respectively.

It is commonly observed with the double-edge-notched and the surface-notched specimens that the extension at fracture increases by adding CB while the maximum tensile load increases by adding MWCNT. Thus, the increases of the fracture toughness by adding CB and MWCNT are caused by different factors, the former being the increase in the extension at fracture of the film and the latter being the increase in the load required to stretch the film.

The increase of the fracture toughness by the addition of CB and MWCNT is larger with the surface-
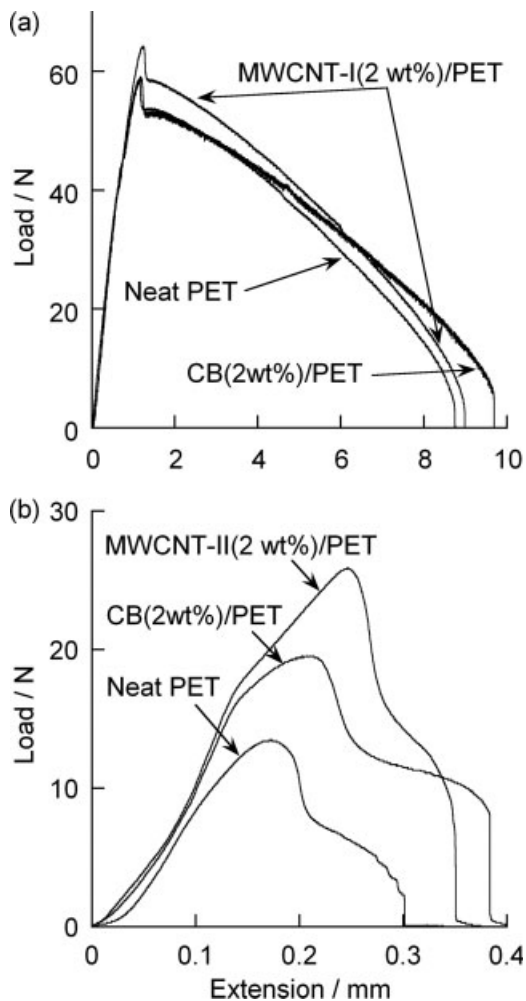
Figure 4 Load-extension curves of neat PET film, CB (2 wt %)/PET composite film, MWCNT-I (2 wt %)/PET composite film, and MWCNT-II (2 wt %)/PET composite film measured using double edge-notched specimens ($L = 17$ mm) (a) and surface-notched specimens (b).

notched specimens than with the double-edge-notched specimens. This difference may be related to the difference in the stress conditions, which causes the difference in the plastic zone shape and size. It is considered that the stress condition in the double-edge-notched specimen is close to the plane-stress state while that in the surface-notched specimen is rather close to the plane-strain state. The plane-strain condition is in favor of the development and growth of the crazes. Thus, the effects of the additions of CB and MWCNT are more emphasized with the surface-notched specimens than with the double-edge-notched specimens. The difference in the stress states also manifests itself in the load-extension curves. The load gradually decreases before fracture with the double-edge-notched specimens whereas it decreases abruptly at the fracture points with the surface-notched specimens. That is, the double-edge-notched specimens fracture in a more ductile manner than the

surface-notched specimens, suggesting that the shear deformation prevails in the former specimens while the crazes are developed more favorably in the latter specimens.

Fracture toughness

Figure 5 shows representative load-extension curves of the double-edge-notched specimens. The area under load-extension curves divided by BL gives the w_t values. Figure 6 shows the plots of w_t against L for the neat PET films, CB (2 wt %)/PET composite films, and MWCNT-I (2 wt %)/PET composite films. The w_t value increases by adding CB and MWCNT-I, especially at a large ligament length.

The values of w_e and βw_p were determined as the intercept and the slope of the regression lines fit to the w_t vs. L plots of the composite films with various filler contents. The results are shown in Figure 7(a,b) as a function of the filler contents. As the fractions of
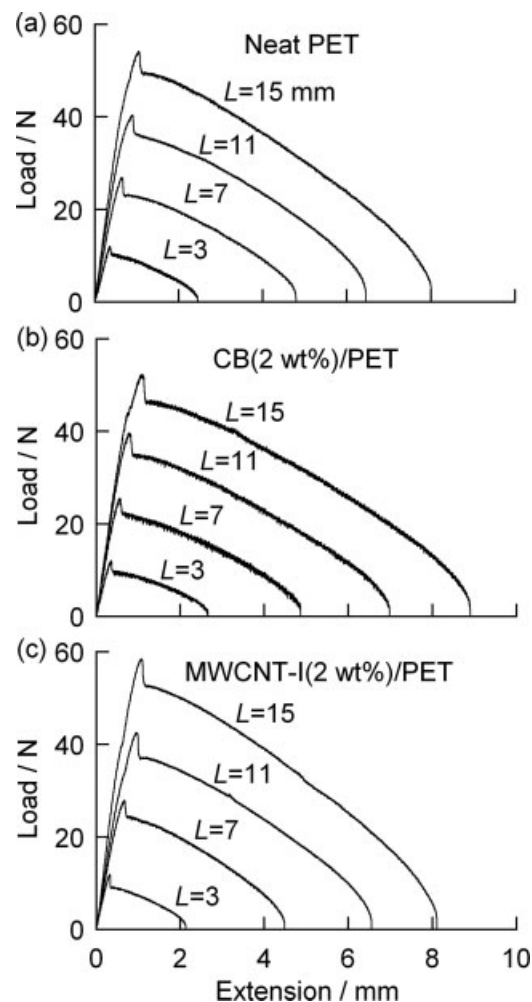

Figure 5 Load-extension curves of neat PET films (a), CB (2 wt %)/PET composite films (b), and MWCNT-I (2 wt %)/PET composite films (c) measured using double-edge-notched specimens with various ligament lengths L shown in the figure.
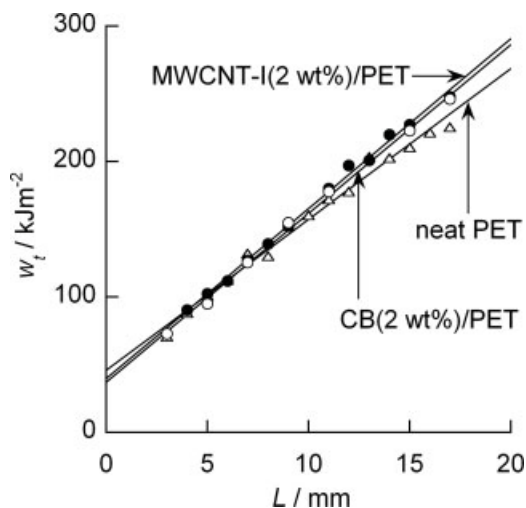
Figure 6 Total work of fracture per unit area w_t for neat PET films (open triangles), CB (2 wt %)/PET composite films (open circles) and MWCNT-I (2 wt %)/PET composite films (closed circles) versus ligament length L.

CB and MWCNT-I increase, w_e decreases at the filler contents from 0 to about 1 wt %, maintained constant values from 1 to about 3 wt %, and decreases again beyond 3 wt %. On the other hand, βw_p increases at the CB contents from 0 to about 3 wt % and at the MWCNT-I contents from 0 to about 2 wt % and decreases thereafter. The initial decrease in w_e is supposedly caused by poor bonding between the fillers and the PET matrix. The later decreases in w_e and βw_p are caused by the filler aggregation as shown in a previous work.[14] From these results, it can be known that the increase in βw_p contributes to the increase in w_t.

Evolution of crazes

The SAXS patterns of the films observed at various characteristic points of the load-extension curves are shown in Figures 8–11. In these figures, the same alphabetical symbols are used to refer to the points with similar characteristics of the load-extension curves. For example, (B) refers to the point at maximum load for any specimen.

When the crazes are formed in the film, a cross-shaped SAXS pattern is developed. The streak in parallel to the loading direction is the total reflection at the craze/polymer interfaces, and the streak perpendicular to the loading direction is the fibril/void scattering. The structure of the crazes can be investigated by analyzing the latter streak.[24,25] In this study, an integrated intensity Q is defined as follows:

$$Q = \iint 2\pi I(s_1, s_2) s_2 ds_2 ds_1 \qquad (5)$$

where $I(s_1, s_2)$ is the intensity distribution of the fibril/void scattering and s_1 and s_2 are the compo-

nents of the scattering vector in parallel and perpendicular to the loading direction, respectively. The value of Q is in portion to the total volume of the fibril/void structures, the electron density difference between the fibrils and the void, and $v(1 - v)$ where v is the volume fraction of the fibrils (or the voids) in the fibril/void structure. Therefore, Q value increases with the increase in the number and/or the length of the fibrils aligned in parallel to the loading direction. When the fibrils break, they may spring back to some bent or wavy forms and the vacant spaces left behind do not contribute to SAXS. Thus, the Q value decreases when the crazes turn into the true cracks. In this study, the Q values were obtained by performing the integration of eq. (5) in the region of $|s_1| < 0.011$ and $0.025 \text{ nm}^{-1} < s_2 < 0.1 \text{ nm}^{-1}$. For the composite films, the scattering of the fillers was subtracted from the measured intensity distributions before integration. This was done by scanning each
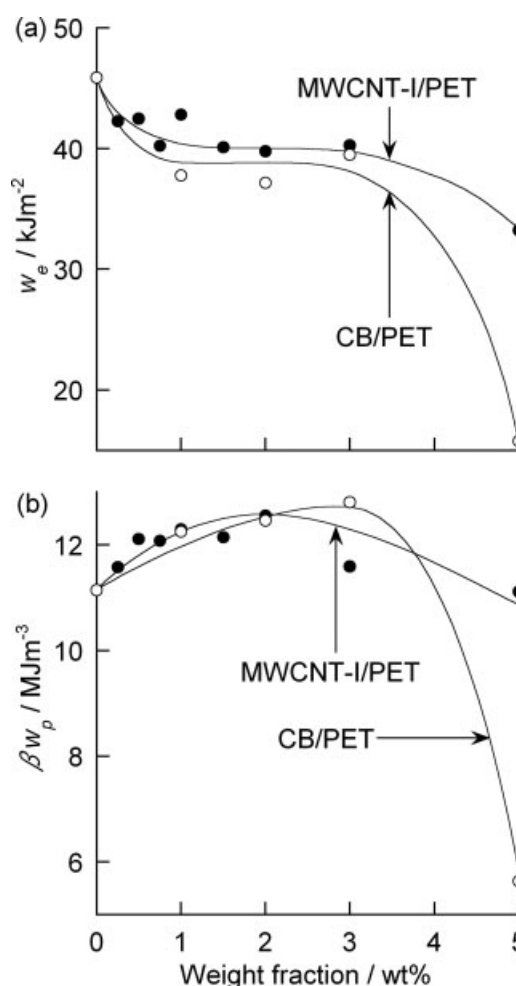

Figure 7 Essential work of fracture per unit area w_e (a) and product of plastic work of fracture per unit volume w_p and plastic zone factor β (b) for CB/PET (open circles) and MWCNT-I/PET (closed circles) composite films versus weight fraction of fillers.
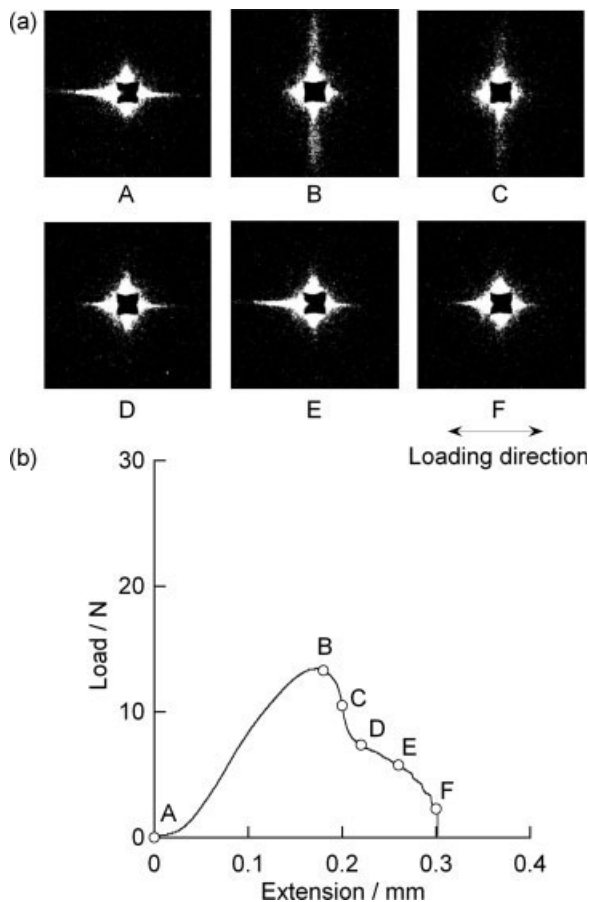
Figure 8 Selected SAXS patterns of neat PET film (a) and at characteristic points of load-extension curve (b).

SAXS pattern at an angle of 45° against the loading direction and regarding this profile as the intensity distribution of the fillers. In this experiment, the incident beam was collimated using the slits in parallel and perpendicular to the loading direction and the parasitic scattering from these slits appears in the SAXS patterns in parallel and perpendicular to the loading direction. This causes nonzero value of Q even before tensile deformation. This nonzero value was subtracted from the values of Q for the specimen under deformation.

The Q values of the films are shown in Figure 12 as a function of the extension together with the load-extension curves. The variations of Q with increasing extension of the films differ considerably among the neat PET film, CB/PET composite film, and MWCNT/PET composite films. For the neat PET film, the Q value starts to increase rapidly at a small extension of about 0.10 mm, reaches maximum at the maximum load and abruptly decreases to zero thereafter. For the CB (2 wt %)/PET composite film, the Q value starts to increase at a much larger extension of about 0.22 mm at which the load starts to decrease and then continues to increase up to the fracture of the film. The Q value of the MWCNT-I (1 wt %)/PET and

MWCNT-II (2 wt %)/PET composite films increase markedly at an extension of about 0.2 mm. The Q value of these films turns to decrease at the maximum load but does not decrease to zero unlike the neat PET film.

The major difference in the variations of the Q values between the neat and the composite films is that the Q value of the neat film abruptly decreases to zero concomitantly with the decrease of the load of the film while that of the composite films does not. On the basis of the hypothesis that the crazes turn into the true cracks when the fibrils reach to a certain critical length and break, the difference of the fracture behavior between the neat and the composite films is considered to be brought about by the difference whether the increase in the external extension promotes the growth of the crazes formed at earlier stages of tensile deformation or creates new crazes. If the crazes formed at earlier stages grow predominantly without being accompanied by the formation of the new crazes, the fibrils in these crazes reach to the critical length at a small external extension. This is the case with the neat PET film. On the other hand, if the new crazes are formed during tensile deforma-
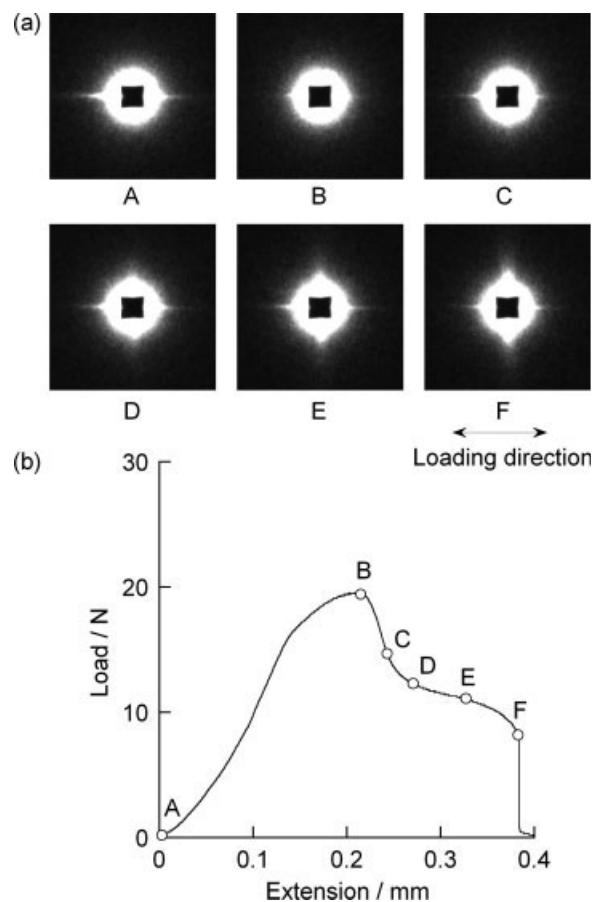

Figure 9 Selected SAXS patterns of CB (2 wt %)/PET composite film (a) at characteristic points of load-extension curve (b).
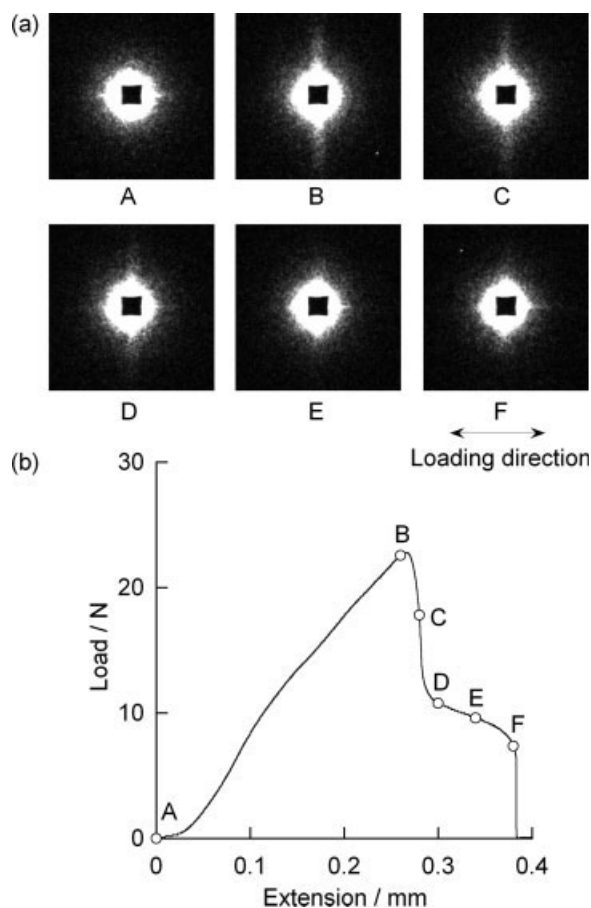
Figure 10 Selected SAXS patterns of MWCNT-I (1 wt %)/ PET composite film (a) at characteristic points of load-extension curve (b).

composite film, the crazes are formed in microscopically polymer-rich regions of the film. When the crazes formed at earlier stages increase their length and the craze tips reach to the regions where MWCNT exists, the energy needed to widen the crazes is increased due to the bridging effect of MWCNT. This promotes the formation of new crazes in other regions and avoids the localization of deformation upon the crazes formed at earlier stages. This bridging effect arises from the large aspect ratio of MWCNT.

CONCLUSIONS

CB and MWCNT increases the fracture toughness of the PET film by increasing the plastic work of fracture. This comes from the effect of the fillers to prevent the localization of deformation upon the crazes formed at earlier stages of tensile deformation and to retard the growth of the fibrils to a critical length. In the case of CB, the CB particles dispersed over the entire specimen volume provide a number of sites where the crazes are preferably formed due to stress
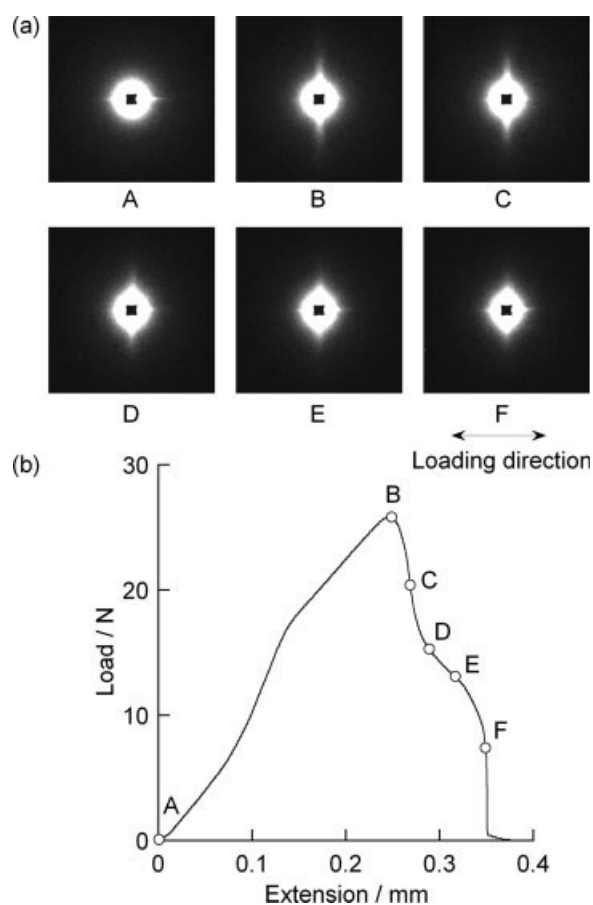
tion, deformation is not localized upon the crazes formed at earlier stages but shared between the crazes formed at various stages, and the fibrils break at much larger external extension. This is the case with the composite films. Although both of CB and MWCNT cause the increase of fracture toughness, they do so in different manners. That is, CB increases the extension at fracture of the film while MWCNT increases the load required to stretch the film. This suggests that the CB particles provide a number of sites where crazes are preferably formed while MWCNT increases the resistance against the widening of the crazes. It is considered that in the CB/PET composite film, the crazes are formed around the CB particles due to stress concentration. The CB particles dispersed over the entire specimen volume provide a number of sites where the crazes are preferably formed and prevent the localization of deformation upon the crazes formed at earlier stages. It is considered that the small crazes formed in the CB/PET film at early stages do not have the regularly aligned extended fibril/void structure and they do not contribute to SAXS. In the case of the MWCNT/PET

Figure 11 Selected SAXS patterns of MWCNT-II (2 wt %)/ PET composite film (a) at characteristic points of load-extension curve (b).
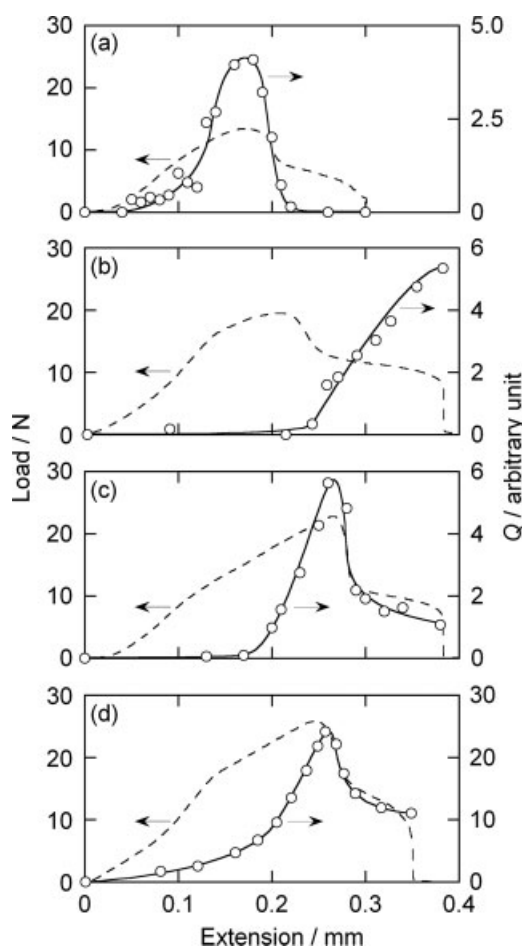
Figure 12 Integrated intensity Q (circle) and load of film (broken line) versus extension of film for neat PET film (a), CB (2 wt %)/PET composite film (b), MWCNT-I (1 wt %)/PET composite film (c) and MWCNT-II (2 wt %)/PET composite film (d).

concentration. In the case of MWCNT, the widening of the crazes formed at earlier stages is suppressed due to the bridging effect of MWCNT. The addition of CB increases the extension at fracture of the film while the addition of MWCNT increases the load required to stretch the film. The bridging effect of the MWCNT arises from the large aspect ratio of MWCNT.

References

 1. Overney, G.; Zhong, W.; Tománek, D. Z. Phys 1993, D27, 93.
 2. Lu, J. P. Phys Rev Lett 1997, 79, 1297.
 3. Hernández, E.; Goze, C.; Bernier, P.; Rubio, A. Phys Rev Lett 1998, 80, 4502.
 4. Treacy, M. M. J.; Ebbesen, T. W.; Gibson, J. M. Nature 1996, 381, 678.
 5. Wong, E. W.; Sheehan, P. E.; Lieber, C. M. Science 1971 1997, 277.
 6. Yu, M.; Lourie, O.; Dyer, M. J.; Moloni, K.; Kelly, T. F.; Ruoff, R. S. Science 2000, 287, 637.
 7. Qian, D.; Dickey, E. C.; Andrews, R.; Rantell, T. Appl Phys Lett 2000, 76, 2868.
 8. Enomoto, K.; Yasuhara, T.; Kitakata, S.; Murakami, H.; Ohtake, N. New Diamond Frontier Carbon Technol 2004, 14, 11.
 9. Satapathy, B. K.; Weidisch, R.; Pötschke, P.; Janke, A. Macromol Rapid Commun 2005, 26, 1246.
10. Tang, W.; Santare, M. H.; Advani, S. G. Carbon 2003, 41, 2779.
11. Gorga, R. E.; Cohen, R. E. J Polym Sci Part B: Polym Phys 2004, 42, 2690.
12. Coleman, J. N.; Cadek, M.; Blake, R.; Nicolosi, V.; Ryan, K. P.; Belton, C.; Fonseca, A.; Nagy, J. B.; Gun'ko, Y. K.; Blau, W. J. Adv Funct Mater 2004, 14, 791.
13. Ye, H.; Lam, H.; Titechenal, N.; Gogotsi, Y.; Ko, F. Appl Phys Lett 2004, 85, 1775.
14. Kobayashi, H.; Shioya, M.; Tanaka, T.; Irisawa, T. Compos Sci Technol, in preparation.
15. Cai, H.; Yan, F.; Xue, Q. Mater Sci Eng A 2004, 364, 94.
16. Allaoui, A.; Bai, S.; Cheng, H. M.; Bai, J. B. Comp Sci Technol 1993, 2002, 62.
17. Ren, Y.; Li, F.; Cheng, H. M.; Liao, K. Carbon 2003, 41, 2177.
18. Gojny, F. H.; Wichmann, M. H. G.; Köpke, U.; Fiedler, B.; Schulte, K. Comp Sci Technol 2004, 64, 2363.
19. Bhattacharya, S. K. Polym Commun 1984, 25, 10.
20. Mark, J. E. Prog Polym Sci 2003, 28, 1205.
21. Efimov, A. V.; Shcherba, V. Y.; Bakeyev, N. F. Polym Sci 1991, 33, 568.
22. Shioya, M.; Kawazoe, T.; Kojima, J.; Sakurai, S.Polymer Processing Society Asia/Australia Meeting, Abstracts, Gyeongju, Korea, 2004; CD-ROM.
23. Kramer, E. J. Polym Eng Sci 1984, 24, 761.
24. Kramer, E. J. Adv Polym Sci 1983, 52/53, 1.
25. Kramer, E. J.; Berger, L. L. Adv Polym Sci 1990, 91/92, 1.
26. Cotterell, B.; Reddel, J. K. Int J Fracture 1977, 13, 267.
27. Hashemi, S.; Yuan, Z. Plast Rubber Proc Appl 1994, 21, 151.
28. Hashemi, S. J Mater Sci 1997, 32, 1563.
29. Ruland, W. Acta Crystallogr 1961, 14, 1180.
30. Sotton, M.; Arniaud, A.; Rabourdin, C. J Appl Polym Sci 1978, 22, 2585.
31. Valentini, L.; Biagiotti, J.; Lopenz-manchado, M. A.; Santucci, S.; Kenny, J. M. Polym Eng Sci 2004, 44, 303.
32. Mucha, M.; Marszałek, J.; Fidrych, A. Polymer 2000, 41, 4137.